Contents lists available at ScienceDirect

Polymer

journal homepage: www.elsevier.com/locate/polymer

Scattering of X-rays during melting and solidification of thermoplastic polyurethane. Graphite as nucleating agent and stabilizer of the colloidal melt

Almut Stribeck[a*], Raphaël Dabbous[b], Berend Eling[a,c], Elmar Pöselt[c], Marc Malfois[d], Edgar Schander[c]

[a]Institute of Technical and Macromolecular Chemistry, Bundesstr. 45, 20146 Hamburg, Germany.
[b]BASF Schweiz AG, WKA 4047.Z.08, Hardmattstr. 434, CH-5082 Kaisten, Switzerland
[c]BASF Polyurethanes GmbH, Elastogranstr. 60, D-49448 Lemförde, Germany
[d]ALBA Synchrotron Light Source, Cerdanyola del Vallès, Catalonia, Spain

ARTICLE INFO

Article history:
submitted: 6 June 2018
revised: 6 August 2018
accepted:
26 August 2018

Keywords:
Polyurethane
Solidification
Scattering

ABSTRACT

Melting and solidification of thermoplastic polyurethanes (TPU) are monitored by X-ray scattering. The colloidal character of the typical material becomes unstable as soon as the hard domains (HD) are molten. Then the scattered intensity fluctuates considerably and "lost" photons are found at small scattering angles (Tyndall effect). In this temperature regime the material is a fluid. Competing homogenization and segregation processes appear to take place, which modulate the materials colloidal character.
Monitored by SAXS and WAXS, TPU elastomers are melted and re-solidified (heating rate: 20 K/min, temperatures T_{max}: 220 °C, 190 °C). Strong fluctuations in scattering intensity due to varying Tyndall effect are observed in most of our experiments. Here the typical effects are demonstrated on a polyether-based TPU with a hard segment content of 30%, whose colloidal melt is stabilized by adding 0.5% graphite. In the hot quiescent melt the morphology is characterized by density undulations. HD arrangement does not grow late. Graphite stabilizes the colloidal melt. It increases both the HD melting-temperature (from 185 °C to 210 °C) and the HD formation temperature (from 90 °C to 165 °C).

1 Introduction

Examining different polymeric materials, one will find a wide range of morphologies. Their spectrum ranges from single-phase, fully amorphous materials to multi-phase materials. The hardness and domain size of these phases as a function of temperature often determines their suitability for an application. The formation of these phases is significantly influenced by the temperature profile in the production, additives and the chemical structure of the polymer chain. For homopolymers, morphology formation appears better understood than for block copolymers. In particular, the complicated morphology formation of the random urethane block copolymers [1] still eludes a sufficient description. If one had the appropriate understanding, one could predict the morphology as well as the properties of such multiphase materials on the basis of the chemical structure and the production parameters [2].

Also in the case of thermoplastic polyurethanes (TPUs), the lengths of the hard blocks vary considerably. Despite this heterogeneity, solidifying forms hard domains. They are essential to the desired properties. From the fluid of the well-mixed melt, the solid multiphase material is formed on cooling. We are interested in the mechanisms behind it – and thus in the relationship between the chemical structure and morphology arising. Simplifying the chemical structure of polyurethanes, we define as segments the repeatable units along the polymer chain. Blocks in the chain are sequences of identical segments. They are terminated by segments of a different kind. A domain is a particle in the material formed from blocks of the same kind.

Even the perfect melt of a TPU lacks the homogeneity of the melt of a homopolymer because the TPU melt consists of

*Corresponding author. E-mail address: almut@stribeck.de

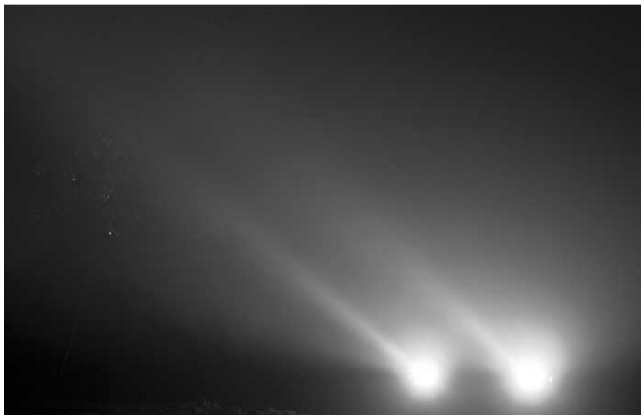

Figure 1. Effect of a colloid to light passing through it

hard and soft blocks. The TPU melt has a pronounced colloidal character, because the hard blocks can be understood as filaments floating in a fluid of different density. By analogy with the terrestrial atmosphere, the melt of a homopolymer is more like clear air whereas block copolymer melts resemble a mist. During solidification, the filamentous blocks form compact domains. Only in the simplest case does the colloidal character of the melt change neither before nor during solidification.

Moreover, in a random block copolymer which contains blocks of distinguishable length one can imagine observing even several distinguishable processes which change the character of the colloid prior to solidification or simultaneously. Such a process may be explained by a segregation mechanism, e.g. a demixing of the melt. Chain pieces of similar sequence structure segregate within the fluid and form some kind of drops. Inside such drops the hard segments would be pre-sorted, because only similar hard-block lengths would be found inside a drop, and also the hard-segment content inside a drop would differ from the respective value in the surrounding.

A fluid exhibits colloidal character when it has significant fluctuations in density. In soft matter, the density fluctuations are much greater than, e.g. in metallic materials. Nevertheless, in materials science the colloidal nature of soft matter is rarely considered. We neglect it because the colloidal structure of the sample usually changes only slightly during the experiment. On the other hand, if the colloidal character of the sample changes significantly, we trust that we will not overlook the corresponding information in the measured data. If we collect scattering data, then our confidence can be great, because the scattering method distinguishes sensitively between a liquid and a colloid. In the scattering only the colloid shows the Tyndall effect. We know its consequences from daily experience (Figure 1). Only a colloid makes the (X-ray) light source appear blurred when we look into the headlamp. In addition, there is a scattering background: the light beam itself is visible from a range of angular directions as it penetrates a colloid. If we drive through wafts of mist at night, then the changing fog modulates both the forward scattering and the background scattering. The shape change of the primary beam is reported in the literature e.g. using the term "multiple scattering" [3–10]. The background scattering is caused by the interaction with short-range density fluctuations as described by Smoluchowski [11] and Einstein [12]. However, the wavelength of X-rays is much smaller than the wavelength of visible light, and the average size of the inhomogeneities is much bigger than the X-ray wavelength. As the wavelength decreases, so does the angular range in which the described effects occur. Thus the widening of the primary beam is found in the ultra-small-angle X-ray scattering regime, and the isotropic part of the Tyndall-effect visible-light scattering becomes the density fluctuation background [13–16] of the small-angle X-ray scattering (SAXS). Finally, the photons consumed by the Tyndall effect are both missing to illuminate the morphology and to probe it. We have carried out many scattering experiments on the formation of structure in elastomeric TPUs during melt solidification and frequently we have observed the characteristic features of a varying colloidal structure.

Beyond phenomenology, there are some questions that are of importance to materials science. First of all, it appears interesting to characterize the temperature range in which such complex variations occur. What do they teach us about the mechanisms that become effective and about the states that the material undergoes during melting and solidification? Why do several competing mixing or segregation mechanisms become effective when such random block copolymers are melted or solidified? In order to approach the answers to some of these and other questions, additional studies will probably be needed. For this first report we have selected a small set of experiments. It not only demonstrates the effect, but also provides new insight into the influence of graphite on the morphology evolution of a polyether-based, elastomeric TPU.

2 Material

The neat material is a TPU made by BASF Polyurethanes GmbH, Lemförde, Germany. Its hard segment content (HSC) is 30%. It is based on a polyether with soft segments from polytetrahydrofurane (PTHF1000®). The diisocyanate is methylene diphenyl diisocyanate (MDI). The chain extender is 1,4-butanediol (BD). The material is injection molded by BASF. Samples of 2 mm thickness are studied. Small disks are cut from the centers of the injection molded plates. They are annealed for 20 h at 100 °C the day before the experiments at the synchrotron and sealed in aluminum foil. This is done both to diminish water uptake and to support the molten material.

A second sheet of the material is graphitized (0.5 wt.-%).

3 Experiments

Melting and solidification. Heat treatment is carried out in a Linkam® hot stage MDSG600 provided with a liquid-nitrogen cooler. Before the start of the measurement the tem-

perature is equilibrated at 40 °C. A constant heating rate of 20 K/min is applied until $T_{max} \in [220\,°C, 190\,°C]$ is reached. The sample is kept at T_{max} for 15 s. Then it is cooled applying a cooling rate of 20 K/min. The highest T_{max} is determined in a test run by monitoring the X-ray absorption. It is chosen 10 K below the temperature at which the absorption is lowered considerably because the material flows down in its sample bag. Discussed temperatures are rounded to the nearest 5 °C.

The aperture of the sample holder begins to shade the wide-angle scattering for d-spacings below 1.25 Å.

Synchrotron setup. Experiments are carried out at the Spanish synchrotron radiation facility ALBA at beamline BL11-NCD using a wavelength of 0.1 nm. The X-ray primary beam at the sample position is 350 µm wide and 380 µm high.

SAXS is collected by a two-dimensional (2D) PILATUS® 1M detector (DECTRIS, Switzerland) placed in a distance of 6.6 m of the sample. In our setup the detector registers d-spacings between 110 nm and 2.75 nm.

WAXS is collected using a 2D Rayonix® LX-255 detector. The detector has 1920×5760 pixels of size $44\,\mu m \times 44\,\mu m$. Its high resolution makes it possible to easily separate the sharp reflections of the aluminum wrapping from peaks of the thick polymer sample. The vacuum tube for the SAXS is guided through a notch in the WAXS detector, as the WAXS detector looks around the tube. The WAXS detector is tilted, and the distorted recorded pattern is de-skewed and calibrated by on-site software. The detector registers d-spacings between 8.8 Å and 0.75 Å, but the aperture of the sample holder limits the maximum scattering angle as already mentioned.

The materials of the present study had also been used in feasibility studies carried out at the synchrotrons in Stanford, USA (SSRL, BL1-5) and in Hamburg, Germany (DESY, beamline P03). There only SAXS had been available, but T_{max} had been higher. At SSRL the temperature resolution had been too low, at DESY the furnace had worked in an unstable equilibrium and had been difficult to control. Moreover, we had destroyed the oven in one of the experiments running to a $T_{max} = 240\,°C$. The data from the successful experiments are taken into account in the discussion of the effect of T_{max}.

Environment tracking. Every snapshot ("frame") is accompanied by a set of environmental data. The synchrotron current itself is a low-noise measure of the intensity $I_{1,f}$ of the incoming primary beam, because ALBA runs top-up mode. The intensity of the transmitted beam, $I_{2,f}$ must be recorded individually for every frame using a PIN-diode in the primary beam stop. These data serve the normalization for constant incident flux and constant sample thickness.

The machine background scattering is recorded with two aluminum foils in the sample holder. The foils contribute the effect of the sample wrapping. Together with the machine background the two quantities $I_{1,b}$ and $I_{2,b}$ of the machine background are recorded. The background determination is repeated several times to assess the noise of the PIN-diode readings in $I_{2,b}(i)$, $i = 1 \ldots 20$.

The sample temperature reported by the Linkam® MDSG600 is saved with each frame. It follows the specified temperature program without significant deviation.

Monitoring the heat treatment. Scattering patterns are registered every 3 s ($\Delta T = 1K$) with an exposure of 2 s. All the patterns are isotropic and are reduced to scattering curves before analysis.

4 Data evaluation

4.1 Computing

Computer program code is ported from licensed or old-fashioned programming environment to Python. The result is a wrapper program SASkia [17] ("small-angle scattering kit for interpretation and analysis"). It supplies commands for the processing of curves. The program can easily be extended by external Python scripts. Related to the presented study such scripts are used, e.g. to read foreign data formats or to concatenate curves side-by-side into 2D patterns and to process them. Program and scripts are available from A.S. on request. SASkia is developed to run under Python 2 and Python 3. Provisions are made to have SASkia run under both Linux and MS-Windows (in an Anaconda environment). The interactive graphics runs smoothest under Python 2.7.

4.2 Preprocessing

Sample transmission. The background data $I_{2,b}(i)$ exhibit statistical noise of ±10%. The raw transmission data $I_{2,f}(f)$, $f = 1 \ldots 365$ during the experiments show similar noise. At low temperature the reading fluctuates about a constant value, and in the melt the smoothed $I_{2,f}(f)$ increases slowly. This is readily explained by the observed slight thinning of the irradiated region of the sample due to gravitational viscous flow. The curves $I_{2,b}(i)$ and $I_{2,f}(f)$ are smoothed yielding the value $\bar{I}_{2,b}$ and the curve $\bar{I}_{2,f}(f)$. Using the smoothed data avoids injection of the PIN-diode noise into the time line of the experiment. Consequently, the transmission coefficient c_t is approximated for each frame f by

$$c_t(f) \approx \frac{\bar{I}_{2,f}(f)\, I_{1,b}}{I_{1,f}(f)\, \bar{I}_{2,b}}. \tag{1}$$

Using the relation

$$c_t = \exp(-\mu t_m) \tag{2}$$

and the assumption that the linear absorption coefficient μ does not change during the experiment, the scattering of each frame is corrected for zero absorption and constant sample thickness t_m. The intensities are calibrated to absolute units using a polypropylene standard of known scattering power. Because of the Tyndall effect we refrain from discussing the absolute values.

WAXS data preprocessing. Only the WAXS is affected by the diffraction from the aluminum wrapping. In the WAXS curve each aluminum spike appears twice, namely from each the front and the back foil of the sample wrapping. Thus the distance Δs_t between twinned aluminum peaks is a footprint of the unavoidable smearing of each WAXD feature. Consequently, a median filter of width $\Delta s_t/2$ applied to the curve removes all the Al-peaks without affecting possible diffraction peaks of the sample.

Background subtraction. The machine background is subtracted from each corrected frame.

4.3 Trend visualizations

Curve of total WAXS. If $I_{WAXS}(s)$ is the WAXS curve obtained so far, a convenient curve for further assessment is

$$I_{W,Q}(s) = 4\pi s^2 I_{WAXS}(s). \tag{3}$$

Here $s = (2/\lambda)\sin\theta$ is the modulus of the scattering vector with the scattering angle 2θ and λ the wavelength of the radiation. From a practical point of view this representation enhances smaller effects in the tail of the scattering. Applied to the scattering of polymers, this curve exhibits the different orders of the amorphous halo. In the case of our polymer this curve shows that the second order of the amorphous halo ends at $s_{h2} \approx 8\,\mathrm{nm}^{-1}$, just before the aperture of the sample holder starts to shade the WAXS intensity. From the theoretical point of view its integral

$$Q_W = \int_0^\infty I_{W,Q}(s)\, ds \tag{4}$$

counts all the electrons which contribute to the WAXS [18–20] – if only the incoherent background can be subtracted. According to Ruland [19, 21] the incoherent background is a well-defined constant c_C. Only to estimate if the WAXS is subjected to absorptive loss during the time of our experiment, we approximate $c_C \approx I_{WAXS}(s_{h2})$ and obtain the representation

$$I_{W,total}(s) \approx 4\pi s^2 \left(I_{WAXS}(s) - I_{WAXS}(s_{h2})\right). \tag{5}$$

Anticipated, in the melt many experiments show fluctuating damping and recovery of the curve $I_{W,total}$ as a whole. In this context it is important to mention that the most obvious reason for an artifact can be excluded, because such variation is not induced by an opposing trend of c_C. On the contrary, whenever $I_{W,total}$ is dampened, then $c_C = I_{WAXS}(s_{h2})$ is likewise attenuated.

Visualization of the SAXS. According to scattering theory photons which are lost in the WAXS must show up in a different regime of scattering. In order to visually inspect, if some of these photons are found in the SAXS, a logarithmic representation of the SAXS intensity $I_{SAXS}(s)$ appears to be appropriate. It maps the intensity curve to a plot, in which changes at both ends of the SAXS curve easily catch the eye.

First, in $\log(I_{SAXS}(s))$ the high intensity blurring of the primary primary beam [6] becomes visible, which is typical for the multiple scattering in a colloid. In order to be able to find this effect, the SAXS detector must also detect at sufficiently small scattering angles.

Second, the logarithmic scaling enhances also variations of the background scattering in the tail of the SAXS, where the scattering is dominated by the density fluctuation scattering of the colloid. In order to record the fluctuation background, the SAXS detector must be large enough.

4.4 Quantitative analysis of the SAXS

In analogy to previous work [22–24] on TPU materials, the SAXS is analyzed quantitatively with respect to its information concerning the evolution of the two-phase morphology. The isotropic scattering curves are transformed into two fundamentally different real-space representations of the morphology, $g_1(r)$ and $g(r)$. A computation of Ruland's interface distribution function [25] (IDF) $g_1(r)$ from isotropic SAXS is only reasonable, if the hard and the soft domains are lamellae. In the present studies this assumption leads to IDFs which are physically meaningless. Thus the hard domains are more like grains than layers. Chord distributions (CD) $g(r)$ after Méring and Tchoubar [26, 27] only assume that the material can be approximated by two phases of different density. In our case these are the density of the hard domains and that of the soft phase matrix. The CDs appear physically meaningful and fittable by morphological models.

A CD is computed by projecting [28, 29] the scattering curve $I(s)$ from 3D reciprocal space down to the 1D space by the Abel transform [30, 31] applied twice in succession. The resulting curve $\{I\}_1(s)$ is then multiplied by s^2 to reflect the 1D Porod law [32] and converted into the interference function $G(s)$ by spatial frequency filtering [33]. Spatial frequency filtering is suitable for the processing of big data, because it runs automatically without user intervention.

The morphology of TPUs is very poor. It can be described by very simple structural models [22–24, 34, 35], which at the most take into account correlations of hard domains with a next neighbor ("duo"). A second component considers such hard domains which are placed at random ("solo"). Only the duos make the SAXS long period. For the present melting-solidification studies the most simple model of this class yields very good fits. It contains each one solo component and one duo component. In the model the two components are coupled by the restriction that the domain-size distribution of all hard domains is the same, regardless of whether a domain belongs to the solo component or to the duo component.

The fit returns the following parameters of physical meaning. $a(T)\, v_h$ is the product of the total volume filled by hard domains multiplied by a function $a(T)$ which is governed by the square of the contrast between hard-domain density and soft-domain density. $a(T)$ is supposed to increase with increasing temperature T. The supposition appears reasonable, if the thermal expansion coefficient of the soft matrix is higher

than that of the hard domains. Thus at high temperature the returned value overestimates the amount of remaining hard domains. In analogy, $a(T)\ v_{duo}$ is an approximate measure of the volume fraction of the arranged domains which generate the SAXS long period. Related to the parameters directly defined in the model function, $a(T)\ v_h = (W_{solo} + W_{duo})\,\overline{d}_h$ with W_i being the weight parameters of the fit [22,24]. The "diameter" $\overline{d}_h$ is, in fact, the number-average chord length of a hard domain. Similarly, $\overline{d}_s$ is the average diameter of the soft phase between arranged hard domains. Thus the number-average long period is $\overline{L} = \overline{d}_h + \overline{d}_s$. $\sigma_h/\overline{d}_h$ is the relative standard deviation of the distribution of hard-domain diameters. In similar manner $\sigma_s/\overline{d}_s$ quantifies the relative variation of the soft domain chords between two arranged hard domains.

A single experiment comprises 365 curves $g(r,f)$ with f symbolizing the frame index. In a first round of model fitting each curve is supplied with a standard set of starting parameters. This set is improved in three consecutive regression runs by the Simplex method [36]. As described in earlier work of one of us [33] the algorithm is extended by one step of the Levenberg-Marquardt algorithm in order to be able to assess the quality of the fit, as is described by Draper and Smith [37]. As a result, about 20% of the runs will have found an excellent fit characterized by bottom-line "estimated errors of the function" (EEF), $E(f)$. With 365 frames it is impossible to manually feed the other 80% with better starting values for a second round. Thus we implement the following algorithm:

The EEF values of the first round are collected in the curve $E(f)$. Before the second round $E(f)$ is eroded (width of the sliding box: 15 frames) resulting in $E_{\ominus 15}(f)$. Erosion is a standard morphological operator. It sets the function to the minimum of all the box values. As long as the box contains at least the $E(f)$ of a single acceptable fit, $E_{\ominus 15}(f)$ describes the goal to reach for a good fit. Then $ND(f) = E(f)/E_{\ominus 15}(f) - 1$ is a normalized deviation of frame f from a good fit. For a good fit $ND(f) < A$, with an acceptance level A (typically 0.02). We scan $ND(f)$ for the first acceptable fit. The related set of morphological parameters is kept in mind. Then we start an automated improvement round by looping over all frames. If $ND(f) < A$, the parameter set of this good fit replaces the parameters in mind. If $ND(f) > A$, we take the last good parameter set as starting values for the frame with the unacceptable fit and run a set of regressions.

Because the algorithm runs automatically, it is suitable for big data. As a result, a morphological parameter curve like, e.g., $\overline{d}_h(f)$ looks quite smooth. Remaining extreme outliers are removed by a narrow median filter (over 3 frames), and noise is removed by spline smoothing.

A test shows that the sporadic outliers are caused by the limited numerical accuracy of modern cross-platform programming languages (8-byte instead of 10-byte by directly addressing the numerical coprocessor's "extended" data type).

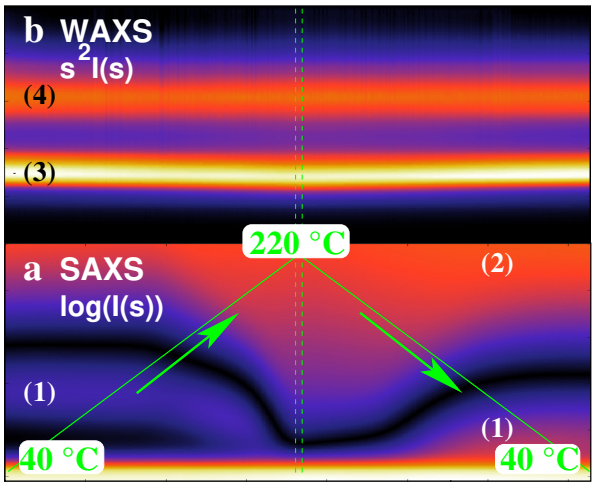

Figure 2. SAXS and WAXS data in a melting-and-solidification experiment. TPU with 0.5 % graphite. The heating and cooling program is indicated in green. (**a**) $\log(I_{SAXS}(s))$ for $0 < s < 0.25\,\mathrm{nm}^{-1}$. (1) indicates the long period peak which vanishes during melting and returns upon solidification. (2) indicates the fluctuation background. Its uniform color shows that the density fluctuations in the material are constant throughout the experiment. (**b**) $I_{W,total}(s)$ for $1 < s < 8\,\mathrm{nm}^{-1}$. The WAXS is constant and only shows (3) the first, and (4) the second order of the amorphous halo

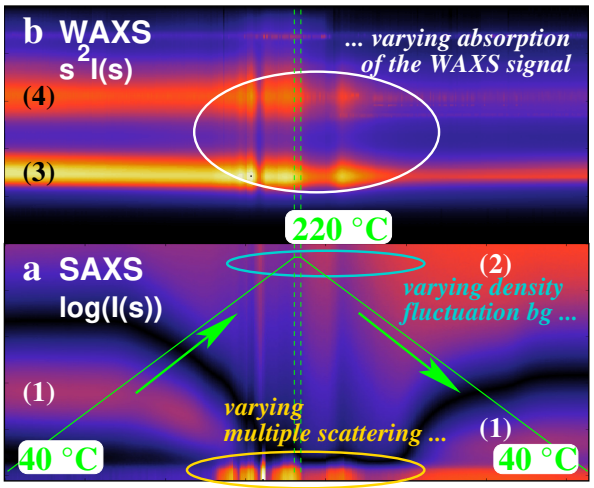

Figure 3. SAXS and WAXS data in a melting-and-solidification experiment (heating rate 20 K/min). Neat TPU shown in the fashion of Figure 2. In addition ellipses indicate (**a**) in the SAXS variations of multiple scattering and density fluctuation scattering; and (**b**) in the WAXS the corresponding loss of WAXS intensity

5 Results and discussion

5.1 Stable and instable colloidal melt

For this first discussion we present the data on different intensity scales. Only in Figures 2 and 3 the highest measured intensity is always the white color. Thereafter, in Figure 4

we will switch to a different scheme, in which all intensities are displayed using the same intensity scale. This has the advantage that intensities can be compared across different runs and materials. The disadvantage is, that then we cannot avoid "overexposed" intensity which leads to cycling the color scheme. In the practice of the present study this only affects very small scattering angles. There we must keep in mind that dark-looking regions do not represent low intensity, but very high intensity. Figure 2 displays the scattering data of the graphitized TPU in the melting-and-solidification experiment. Here already the WAXS intensity $I_{W,total}(s,T)$ is independent of the temperature T. One may be tempted to conclude that here multiple scattering and scattering from density fluctuations are negligible. Instead, as will be shown, it is not small but only constant for this sample in the scanned temperature range.

Figure 3 presents the respective plots for a neat TPU showing early solidification. Here the WAXS exhibits peculiar variations of the intensity, which are accompanied by counterpart variations in the SAXS data below. So it looks as if we have caught a representative fraction of all photons in our two detectors. The photons missing in the WAXS appear in the SAXS. According to repeated experiments this is not the normal behavior of the neat TPU. More frequently, in scattering data from it there is a region in the cooling branch between 150 °C and 90 °C, in which both the SAXS and the WAXS intensity are simultaneously lowered considerably. We discuss this later. Now returning to Figure 2 we see that also the material which contains graphite shows considerable multiple scattering close to the primary beam. Thus the main difference between the two materials is, that in the case of the graphitized material the colloidal structure of the melt does not fluctuate. One might argue that in the case of the graphitized material the high intensity at very small angle may be caused from the ultra-small angle scattering of big graphite particles, and this effect were veiling Tyndall-variations. There are two reasons to assume that this is not the case. First, then at least at higher angles in the SAXS the effect of "varying mist" should show up. Second, with the neat material the Tyndall-broadening of the primary beam (or: multiple scattering) generates very frequently considerably higher absolute intensity than that observed with the graphitized material. There the pseudo-color logarithmic scale does not suffice any more, and the corresponding pixels are in dark color, indicating that a second repeat of the color scale has started.

According to visual inspection, the shape of the amorphous WAXS curves appears unchanged. Closer, individual inspection shows slight movement and widening effects which are explained by thermal expansion.

The graphitized material has no crystal reflections, but in the neat TPU a weak peak is indicated. For demonstration we anticipate Figure 4. In sub-figure A double-head arrow points at the indication of the peak far out in the second amorphous halo at $s_{c1} = 6.95\,\mathrm{nm}^{-1}$, $d_{c1} = 1.44\,\text{Å}$. This peak is not present in the graphitized material (sub-figure D). An ellipse in Figure 4A indicates the melt region above 200 °C, where this peak is more pronounced than at lower temperature. In the experiment with the lower T_{max} (Figure 4C) this region is not reached.

Additionally considering that the colloidal fluid appears only stable in the graphitized TPU, its "amorphous" character may be explained by a mechanism that has been proposed in the introduction. In the stable colloidal fluid of the graphitized TPU any block pre-sorting mechanism prior to solidification is suppressed. In contrast, it appears possible in the dynamic colloid of the neat TPU. After such segregation but still before solidification, the melt would consist of different drops, each mostly containing hard blocks of similar length. Then, predominantly in the drops with long blocks, more perfect hard domains could be formed than comparative domains formed directly from a globally well-mixed melt. Consequently, the graphitized TPU should show less pronounced crystal reflections than the neat TPU, and this is what we observe.

We do not want to exclude that the effect of graphite on the melt may mainly be due to an improvement in the heat conduction. The literature certainly does not give us any further information. There, the interaction between graphite and polyurethane seems to have been discussed mainly in terms of flame retardancy and electrical conductivity.

In summary, visual inspection of the course of the scattering patterns shows that in the neat material strong colloidal mixing/demixing processes start above 190 °C, under which the formation of high-temperature preferring crystallites (HTC) can not be ruled out. If the corresponding WAXD peak is considered significant, some of these HTCs are already present before the experiment – but only in the neat material. The graphitized material neither shows this peak, nor does it exhibit colloidal mixing/demixing processes in the melt, as long as it is only heated to 220 °C (but see Figure 5). The observed effects support the explanation that the high-temperature melting peak found in the DSC of TPU materials may be related to mixing enthalpy [38–40]. It appears unnecessary to postulate the melting of a second polymorph [41–44], but the opposite effect, namely the formation of HTC crystals, can not be ruled out.

5.2 Morphology variation during melting and solidification

In the melt. Density undulations. Figure 4 combines scattering data with the variation of the morphological parameters which are obtained by fitting the solo/duo model to the chord distributions $g(r)$. Now all the pseudo-color images are presented on the same "absolute" intensity scale. Remember, that doing so causes intensity-overflow in some images at ultra-small scattering angle. There a dark region means very high intensity, because the pseudo-color spectrum starts a second cycle. Let us describe what this scaling itself means. "Same scale" means that, first, in all the images the intensity zero is mapped to the color black and, second, the same intensity in units of $\text{e.u.}/\text{nm}^6$, i.e. "electrons per nanometer to the sixth" is mapped to the color white.

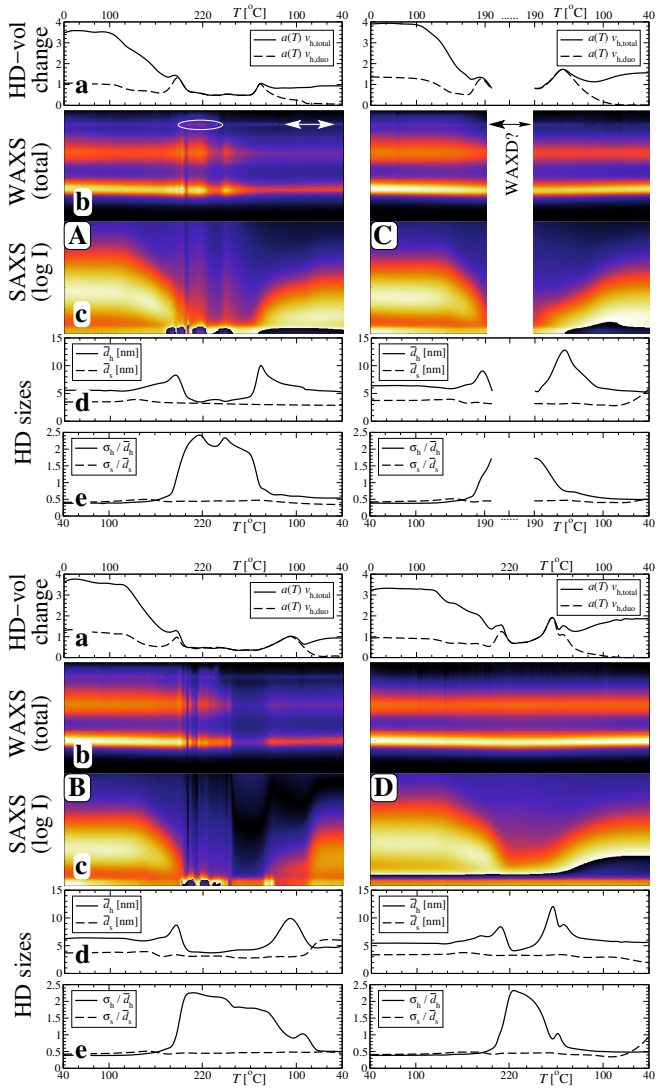

Figure 4. Melting and solidification of a neat and a graphitized TPU. Scattering data and results of morphology analysis. **A**: Neat material, early solidification. **B**: Neat material, late solidification. **C**: Neat material heated only to 190 °C. The arrow above "WAXD?" points at the position at which neat material exhibits a possible crystalline reflection of varying strength. **D**: graphitized material. **a**: volume fractions of hard domains. **b**: Total WAXS intensity curves $I_{W,total}(s)$, $1 < s < 8\,\mathrm{nm}^{-1}$. **c**: SAXS $\log(I(s))$, $0 < s < 0.25\,\mathrm{nm}^{-1}$. **d**: average domain diameters. **e**: widths of the domain-size distributions characterized by their relative standard deviations

Inside each sub-figure A-D, each "row a" shows the global morphology evolution. When heating, the total volume of hard domains decreases strongly. As expected, we also find a faint morphology component in the melt. It appears interesting that not the solo component, but the duo component survives in the melt. Thus, when passing into the melt, the density does not fluctuate statistically, but there are undulations of density which even lead to an increased value of $a(T)\,v_h$. The same happens again when solidifying. The solid state can therefore be characterized in that the solid line $a(T)\,v_h$ extends above the dashed line $a(T)\,v_{duo}$ in each "row a" graph.

In the melt the majority of the "domains" collected in the observed remnant duo component $a(T)\,v_{duo}$ cannot be related to solid hard-domains. This is shown in the solid curves of A and C in "row e": At high temperature the pseudo character of these "domains" is indicated by extremely wide diameter distributions (solid curves). They narrow when solidification sets in. "Row d" shows that in all materials the smaller hard domains melt earlier than the bigger ones.

Neat material: Nuclei, large-scale segregation, and solidification. The sub-figures A, B and C present data from experiments with the neat material. The data in sub-figure A and C show an early solidification: hard domains are formed at 145 °C. In sub-figure B hard-domains are formed later at a much lower temperature of 90 °C. Late solidification is probably the normal behavior of the neat material – provided the temperature of the melt was high enough. This is suggested by the results of two more successful runs on this material collected during previous campaigns. In these campaigns the material had been heated to 240 °C. Early solidification observed in an experiment with lower T_{max} (experiment "D") indicates that early solidification in melts from 220 °C is probably caused from sporadic remnant hard-domain nuclei.

The common, late solidification behavior demonstrated in Figure 4B is accompanied by a broad darkened region in the scattering of the cooling branch between 180 °C and 140 °C. This raises the question of whether we have lost photons. All the experiments on the neat material (A, B, C) share the same constant transmission $c_t(f)$ according to Equation (1). Because the Tyndall effect is mapped on a narrow angular range and we do not find the vanished scattered photons of Figure 4B before they return below 140 °C, they must have been hiding at extremely low angle. A process which can explain this dark zone is a coagulation of hard-segment enriched colloidal particles into much bigger blobs causing scattering at much smaller angle. The process behind this observation is reminiscent of spinodal segregation [45]. Now one might think that this segregation process were linked to the fact that the melt of this sample contains no nuclei. Consulting all our SAXS data from runs of the neat material we find that this is not the case. Moreover, the temperature interval in which it occurs is not constant. In an old successful late-solidification run with a T_{max} of about 240 °C it is observed in [150 °C, 90 °C] instead of in [180 °C, 140 °C]. This could be an indication that also this segregation process is triggered by nuclei specifically related to it.

Also in the heating branches of experiments A and B, we observe dark bands that indicate segregation processes. They are narrow. This may be due to the fact that their activation requires a minimum temperature, but then increasing temperature leads to remixing. We still can not describe the nature of these segregation processes, but they should be swallowed anyway at very high heating rates.

At least the transitions from the solid to the fluid phase and back can be assigned to temperatures based on our measure-

ments. The graphs in "row a" of Figure 4A-C show that in the neat material the hard domains melt at 185 °C, and the start of solidification is found at 145 °C if domain-formation nuclei are present. If no nuclei have survived the melting, the first hard domains are formed at 90 °C.

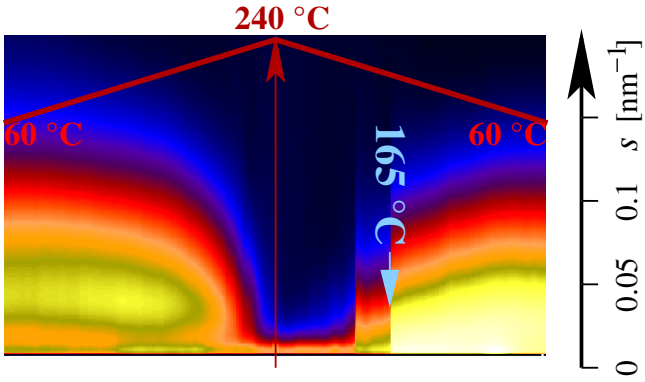

Figure 5. SAXS evolution of the graphitized material in a test run up to $T_{max} = 240\,°C$ (DESY, beamline P03).

Nucleation by graphite. For the graphitized material the transitions from the solid to the fluid phase and back are found at different temperatures according to the respective graphs in Figure 4D. Compared to the neat material the last hard domains melt at a higher temperature of 210 °C, and upon cooling the material solidifies already at 165 °C.

Figure 4 shows that in the neat material ("row a"; subfigures A-C) above 185 °C all the randomly distributed domains are molten. In the graphitized material (D) the last hard domains melt later, at 210 °C. In the cooling branch the graphitized material starts to form hard domains already at 165 °C. This is even earlier than the neat material when it is processed from a melt which still contains nuclei. Thus graphite acts as an effective nucleating agent.

Moreover, graphite appears to stabilize the colloidal structure of the melt at least up to a $T_{max} = 220\,°C$. What happens with a T_{max} of 240 °C, we can partially infer from scattering data recorded in a successful test run at DESY. Figure 5 shows the respective SAXS data. A WAXS detector had not been available. In the SAXS a broad segregation valley is observed between 235 °C in the heating branch and 185 °C in the cooling branch. Between 185 °C and 165 °C some transition happens which may be considered a "pre-formation of morphology", before solidification happens, again, at 165 °C. In the segregation valley the density fluctuation background (intensity at high s) does not change. Thus, exposed to the higher T_{max}, the melt already segregates during heating into a hard-segment-rich phase and a hard-segment-poor phase, without the colloidal character of these two phases changing.

Second-order effects. The hard-domain melting curves of all materials show an indentation around 195 °C. The corresponding hard domains appear to need some extra heat before they vanish. This may be caused from the melting of small crystallites which do not leave a footprint in the WAXS. Nevertheless, such crystallites cannot be the above mentioned HTCs.

The melting-solidification cycle does not change the average dimension of the hard domains, but after the cycle the diameters are somewhat less precisely defined (compare in row e the solid curves at start and end).

6 Conclusions

Based on the presented results and other results which are still unpublished we propose a first approximation to the mechanisms which describe the melting behavior of the studied TPUs. Once the hard domains of the TPUs have melted, the material is in the state of a colloidal fluid, the dynamics of which may cloud or even hide some information about changes of the classical morphology taking place in it. The colloid dynamics manifests itself in the varying Tyndall effect, which indicates that the goal of a homogeneous melt may be difficult to achieve for this group of statistical copolymers under quiescent conditions. In the same way, the phase separation during cooling appears to be aggravated.

It seems that there is no simple solitary process in this random block copolymer that dominates the phase separation. As the fluid cools down, several similarly powerful segregation mechanisms seem to lurk on favorable conditions for them to come to fruition. However, the transition to the solid phase is always characterized by the formation of hard domains. This notion suggests an additional interpretation for earlier results [22] of tensile tests at room temperature. At that time, we found that different TPU materials fail just when all the hard domains have been destroyed by the tensile forces, and based on the results of the present study this appears not only obvious because all the physical cross-links are destroyed, but also because a material without hard domains can be considered fluid.

The observed segregation and mixing phenomena which change the "granularity" of the inhomogeneous fluid are not yet understood. In the heating branch big granules probably are the remnants of the hard domains. In the cooling branch they are found to be their predecessors. So the melt-grains are probably characterized in that their hard-segment density is increased. Inside the big granular blobs even classical morphological processes may take place, e.g. melting or crystallization of the contained hard segments. Apart from such hypotheses, the discrete segregation phenomena observed in the heating branches deserve to be studied by selective annealing and subsequent morphological investigation.

If the polymer melt of a TPU were not inherently a colloid, it would, in any case, become one by the addition of a nucleating agent. The main task of a nucleating agent is to tailor the process of phase separation. But it can also act on the colloidal melt and there it may be able to control the nature of the "colloidal fog" and its stability. However, an observed stabilization of the colloid by a nucleating agent may also simply be a direct consequence of its ability to nucleate.

Of fundamental interest appears also a question about the evolution of morphology: How is the weak order formed that manifests itself in the broad long period reflection of the TPUs? An indication of the answer comes from the quantitative analysis of the SAXS at high temperature. It are not the uncorrelated domains (solos) but the correlated entities (duos) that survive longest in the melt and first arise during solidification. This suggests that the formation of hard domains from the melt is preceded by spatial undulations of density. The statistical character of the copolymer then, on further cooling, probably forces the collapse of the range of these undulations. In contrast to this idea would be the random car-parking process [46]. It is found with several other polymers [47–50]. In this process the domains form at random locations, and correlation only arises late when the last hard domains are parked into the middle of remnant gaps.

Here we report investigations on the quiescent melt. In the industrial process, however, the material is sheared. About the effect of shear on the observed processes we can only speculate. The virgin material has been injection molded and is not oriented. This may be interpreted by the notion that even in the industrial process the melt appears quasi-quiescent what morphology formation is concerned. On the other hand, in the industrially produced sheets, shear-induced orientation could have been destroyed by a randomizing mechanism. Would there be causes other than turbulence for such a mechanism? In any case, we consider turbulence to be unlikely because of the high viscosity of polymer melts as compared to common liquids.

Acknowledgements. The authors are very grateful to Professor Alejandro J. Müller for his valuable suggestions and the fruitful discussion of the manuscript. The experiments have been performed at beamline BL11 - NCD of ALBA Synchrotron with the collaboration of ALBA staff in the frame of project IH-2017072268, "Effect of nucleating agents on melting and solidification of thermoplastic polyurethanes". In particular we have benefited greatly from the support of Juan Carlos Martínez and Eduardo Solano, of the perfect equipment, and of the 24/7 floor service when a thermocouple broke at night.

We are indebted to Karsten Brüning for having carried out a successful feasibility study at the Stanford Synchrotron Radiation Lightsource, beamline BL1-5. At DESY Hamburg, beamline P03, experiments were passionately supported by Wiebke Ohm and Konrad Schneider (IPF Dresden) in two campaigns. K.S. also provided the oven.

References

[1] A. Noshay, J. E. McGrath, Block Copolymers - Overview and Critical Survey, Acedemic Press, New York, 1977, Ch. 7, pp. 371–373.

[2] J. Bicerano, Prediction of Polymer Properties, 3rd Edition, Dekker, New York, 2002, Ch. 19.

[3] R. Hosemann, Röntgeninterferenzen an kolloiden systemen, Kolloid Z. 117 (1) (1950) 13–41. doi:10.1007/BF01525373.

[4] V. Luzzati, Diffusion centrale multiple des rayons x par la matière hétérogène. i. étude théorique, Acta Cryst. 10 (1957) 643–648. doi:10.1107/S0365110X57002248.

[5] R. Perret, W. Ruland, Single and multiple x-ray small-angle scattering of carbon fibres, J. Appl. Cryst. 2 (1969) 209–218. doi:10.1107/S0021889869006996.

[6] R. Perret, W. Ruland, The evaluation of multiple x-ray small-angle scattering, J. Appl. Cryst. 4 (1971) 444–451. doi:10.1107/S0021889871007453.

[7] W. Ruland, H. Tompa, The effect of multiple scattering on structural parameters determined from x-ray small-angle scattering, J. Appl. Cryst. 5 (1972) 1–7. doi:10.1107/S0021889872008623.

[8] J. Schelten, W. Schmatz, Multiple scattering treatment for small-angle scattering problems, J. Appl. Cryst., 13 (1980) 385–390. doi:10.1107/S0021889880012356.

[9] G. R. Mitchell, A. H. Windle, Experimental separation of the coherent component of x-ray scattering prior to rdf analysis of non-crystalline polymers, J. Appl. Cryst. 13 (1980) 135–140. doi:10.1107/S0021889880011740.

[10] M. Gelfer, C. Burger, A. Fadeev, I. Sics, B. Chu, B. S. Hsiao, A. Heintz, K. Kojo, S.-L. Hsu, M. Si, M. Rafailovich, Thermally induced phase transitions and morphological changes in organoclays, Langmuir 20 (9) (2004) 3746–3758. doi:10.1021/la035361h.

[11] M. V. Smoluchowski, Molekular-kinetische theorie der opaleszenz von gasen im kritischen zustande, sowie einiger verwandter erscheinungen, Ann. Phys. 25 (1908) 205–226. doi:10.1002/andp.19083300203.

[12] A. Einstein, Theorie der opaleszenz von homogenen flüssigkeiten und flüssigkeitsgemischen in der nähe des kritischen zustandes, Ann. Phys. 33 (1910) 1275–1298. doi:10.1002/andp.19103381612.

[13] G. Porod, Anwendung und ergebnis der röntgenkleinwinkelstreuung in festen hochpolymeren, Makromol. Chem. 35 (1) (1960) 1–25. doi:10.1002/macp.1960.020350101.

[14] W. Ruland, Small-angle scattering of two-phase systems: Determination and significance of systematic deviations from porod's law, J. Appl. Cryst. 4 (1) (1971) 70–73. doi:10.1107/S0021889871006265.

[15] C. G. Vonk, Investigation of non-ideal two-phase polymer structures by small-angle x-ray scattering, J. Appl. Cryst. 6 (2) (1973) 81–86. doi:10.1107/S0021889873008204.

[16] F. B. Khambatta, F. Warner, T. Russell, R. S. Stein, Small-angle x-ray and light scattering studies of the morphology of blends of poly(ϵ-caprolactone) with poly(vinyl chloride), J. Polym. Sci., Part B: Polym. Phys. 14 (1976) 1391–1424. doi:10.1002/pol.1976.180140805.

[17] A. Stribeck, Saskia - a computer program, www.stribeck.de/saskia (07 2018).

[18] A. Guinier, X-Ray Diffraction, Freeman, San Francisco, 1963.

[19] L. E. Alexander, X-Ray Diffraction Methods in Polymer Science, Wiley, New York, 1979.

[20] B. E. Warren, X-Ray Diffraction, Dover, New York, 1990.

[21] W. Ruland, X-ray determination of crystallinity and diffuse disorder scattering, Acta Cryst. 14 (1961) 1180–1185. doi:10.1107/S0365110X61003429.

[22] A. Stribeck, X. Li, A. Zeinolebadi, E. Pöselt, B. Eling, S. Funari, Morphological changes under strain for different thermoplastic polyurethanes monitored by saxs related to strain-at-break, Macromol. Chem. Phys. 216 (24) (2015) 2318–2330. doi:10.1002/macp.201500255.

[23] X. Li, A. Stribeck, I. Schulz, E. Pöselt, B. Eling, A. Hoell, Nanostructure of thermally aged thermoplastic polyurethane and its evolution under strain, Eur. Polym. J. 81 (2016) 569–581. doi:10.1016/j.europolymj.2015.11.027.

[24] A. Stribeck, E. Pöselt, B. Eling, F. Jokari-Sheshdeh, A. Hoell, Thermoplastic polyurethanes with varying hard-segment components. mechanical performance and a filler-crosslink conversion of hard domains as monitored by saxs, Eur. Polym. J. 94 (2017) 340–353. doi:10.1016/j.eurpolymj.2017.07.020.

[25] W. Ruland, The evaluation of the small-angle scattering of lamellar two-phase systems by means of interface distribution functions, Colloid Polym. Sci. 255 (5) (1977) 417–427. doi:10.1007/BF01536457.

[26] J. Méring, D. Tchoubar, Interprétation de la diffusion centrale des rayons x par les systèmes poreux. i., J. Appl. Cryst. 1 (1968) 153–165. doi:10.1107/S0021889868005212.

[27] D. Tchoubar, J. Méring, Interprétation de la diffusion centrale des rayons x par les systèmes poreux. ii. exemples d'application, J. Appl. Cryst. 2 (1969) 128–138. doi:10.1107/S0021889869006716.

[28] R. Bonart, Kolloidstrukturen in verstreckten hochpolymeren, Kolloid Z. u. Z. Polymere 211 (1-2) (1966) 14–33. doi:10.1007/BF01500205.

[29] N. Stribeck, X-Ray Scattering of Soft Matter, Springer, Heidelberg, New York, 2007. doi:10.1007/978-3-540-69856-2.

[30] N. H. Abel, Auflösung einer mechanischen aufgabe, J. Reine Angew. Math. 1 (1) (1826) 153–157.

[31] R. N. Bracewell, The Fourier Transform and its Applications, 3rd Edition, McGraw-Hill, Boston, 1999.

[32] G. Porod, Die röntgenkleinwinkelstreuung von dichtgepackten kolloiden systemen, Colloid Polym. Sci. 124 (2) (1951) 83–114. doi:10.1007/BF01512792.

[33] N. Stribeck, Utilising spatial frequency filtering to extract nanoscale layer structure information from isotropic small-angle x-ray scattering data, Colloid Polym. Sci. 280 (3) (2002) 254–259. doi:10.1007/s00396-001-0601-z.

[34] N. Stribeck, A. Zeinolebadi, M. Ganjaee Sari, A. Frick, M. Mikoszek, S. Botta, Structure and mechanical properties of an injection-molded thermoplastic polyurethane as a function of melt temperature, Macromol. Chem. Phys. 212 (20) (2011) 2234–2248. doi:10.1002/macp.201100193.

[35] N. Stribeck, A. Zeinolebadi, F. Harpen, G. A. Luinstra, B. Eling, S. Botta, Thermoplastic polyurethane crosslinked by functionalized silica. nanostructure evolution under mechanical load, Macromolecules 46 (10) (2013) 4041–4052. doi:10.1021/ma400512b.

[36] M. S. Caceci, W. P. Cacheris, Fitting curves to data - the simplex algorithm is the answer, Byte 1984 (5) (1984) 340–360.

[37] N. R. Draper, H. Smith, Applied Regression Analysis, 2nd Edition, John Wiley & Sons, New York, 1980.

[38] R. J. Cella, Morphology of segmented polyester thermoplastic elastomers, J. Polym. Sci. - Symp. 42 (2) (1973) 727–740. doi:10.1002/polc.5070420224.

[39] A. Saiani, W. A. Daunch, H. Verbeke, J. W. Leenslag, J. S. Higgins, Origin of multiple melting endotherms in a high hard block content polyurethane. 1. thermodynamic investigation, Macromolecules 34 (26) (2001) 9059–9068. doi:10.1021/ma0105993.

[40] A. Saiani, A. Novak, L. Rodier, G. Eeckhaut, J.-W. Leenslag, J. S. Higgins, Origin of multiple melting endotherms in a high hard block content polyurethane: Effect of annealing temperature, Macromolecules 40 (20) (2007) 7252–7262. doi:10.1021/ma070332p.

[41] J. Blackwell, C. D. Lee, Hard-segment polymorphism in mdi/diol-based polyurethane elastomers, J. Polym. Sci. Part B: Polym. Phys. 22 (4) (1984) 759–772. doi:10.1002/pol.1984.180220417.

[42] L. M. Leung, J. T. Koberstein, Dsc annealing study of microphase separation and multiple endothermic behavior in polyether-based polyurethane block copolymers, Macromolecules 19 (3) (1986) 706–713. doi:10.1021/ma00157a038.

[43] G. Pompe, A. Pohlers, P. Pötschke, J. Pionteck, Influence of processing conditions on the multiphase structure of segmented polyurethane, Polymer 39 (21) (1998) 5147–5153. doi:10.1016/S0032-3861(97)10350-0.

[44] Y. Swolfs, E. Bertels, I. Verpoest, B. Goderis, Linking the morphology of a high hard segment content polyurethane to its thermal behaviour and mechanical properties, Polymer 81 (1) (2015) 1–11. doi:10.1016/j.polymer.2015.11.007.

[45] J. W. Cahn, J. E. Hilliard, Free energy of a nonuniform system. i. interfacial free energy, J. Chem. Phys. 28 (2) (1958) 258–267. doi:10.1063/1.1744102.

[46] A. Rényi, On a one-dimensional problem concerning random space filling, Sel. Transl. Math. Stat. Prob. 4 (1) (1963) 203–218.

[47] E. W. Fischer, Zusammenhänge zwischen der kolloidstruktur kristalliner hochpolymerer und ihrem schmelz-und rekristallisationsverhalten, Colloid Polym. Sci. 231 (1-2) (1969) 458–503. doi:10.1007/BF01500012.

[48] J. W. Evans, Random and cooperative sequential adsorption, Rev. Mod. Phys. 65 (4) (1993) 1281–1329. doi:10.1103/RevModPhys.65.1281.

[49] B. Bonnier, D. Boyer, P. Viot, Pair correlation function in random sequential adsorption processes, J. Phys. A 27 (11) (1994) 3671–3682.

[50] N. Stribeck, Oriented quiescent crystallization of polyethylene studied by usaxs. part 2: The liquid scattering of stacks generated from random placement of lamellae, Macromol. Chem. Phys. 205 (11) (2004) 1455–1462. doi:10.1002/macp.200400034.

Highlights:

- A TPU without hard domains appears as a heterogeneous colloidal fluid
- Generally, temperature variation of the fluid induces mixing and demixing processes
- There are indications that in the fluid even crystals may form
- A nucleating agent may suppress mixing, demixing and crystallization
- Graphite increases the temperatures of hard-domain melting and formation: increased thermal stability